Gravitational Enrichment of ^{84}Kr/^{36}Ar Ratios in Polar Ice Caps: A Measure of Firn Thickness and Accumulation Temperature

H. Craig and R. C. Wiens*

Measurements of ^{84}Kr/^{36}Ar ratios in Greenland ice show that gravitational separation in the firn layer is responsible for the enrichments relative to atmospheric ratios. The ^{84}Kr/^{36}Ar ratio is enriched by 12.8 per mil and is 24 times the ^{18}O/^{16}O enrichment in trapped O_2, as predicted for gravitational fractionation. Because gravitational enrichment depends on firn thickness, which in turn depends on annual mean temperature, noble gas ratios provide a method for determining paleotemperatures and ancient firn thicknesses in polar ice caps. The gravitational effects are modulated by about 10 to 15 percent by atmospheric concentration changes caused by temperature effects on oceanic gas solubilities. The availability of five noble gases should make it possible to deconvolute the solubility and gravitational enrichments for calibration of ^{18}O paleotemperatures throughout the polar ice sheets.

In 1985, Horibe *et al.* (*1*) discovered that O_2 trapped in Greenland ice is enriched in ^{18}O by ~0.6 per mil relative to atmospheric O_2. Craig *et al.* (*2*) showed that this effect could be the possible result of molecular gravitational fractionation in the unconsolidated firn layer above the ice, in which gravitational thermodynamic equilibrium is maintained in what is essentially a thick columnar sieve that prevents convective mixing of the entrained air. ^{15}N and ^{18}O enrichments in air trapped in the upper 100 m of Greenland ice were found to be consistent with the predicted gravitational effects in the firn column (*2*). Because the magnitude of the gravitational effect is a measure of the thickness of the firn layer, measurements of noble gas ratios can be used to establish a history of paleothicknesses of firn layers and their mean accumulation temperatures in polar ice caps.

Firn thickness in the present-day polar ice caps is correlated with ambient firn accumulation temperature (Fig. 1) (*3*); this correlation reflects the strong temperature dependence of the rate of firn-to-ice transition by pressure sintering. Thus, if accurate measurements of gravitational separation effects can be made with the use of gases trapped in polar ice, they will provide a new parameter for the study of past climatic changes. In this report, we present measurements of a noble gas pair with a large mass difference, ^{84}Kr and ^{36}Ar, and show that gravitational separation is indeed the dominant fractionation process.

Gravitational equilibrium for isotope and perfect-gas ratios is described by the Gibbs equation (*4*):

$$R/R_0 = \exp[gZ(\Delta M)/R^+T] \qquad (1)$$

where g is the gravitational acceleration at 65°N, Z is the thickness of the firn layer, R^+ is the gas constant, T is the (isothermal) temperature of the column (in kelvin), $\Delta M = (M_i - M)$ is the mass difference between two isotopes (in atomic mass units), $R(Z)$ is the isotope ratio N_i/N, and R_0 is the corresponding ratio in the free atmosphere at the surface. To first order, the isotope ratio enrichment δ (per mil) is given by

$$\delta \approx 1.180(\Delta M)Z/T \qquad (2)$$

with Z in meters (*5*). Equilibrium gravitational separation thus depends only on the mass difference ΔM between components, rather than on the fractional mass difference ($\Delta M/M$) that governs fractionation by kinetic processes such as effusion (*6*).

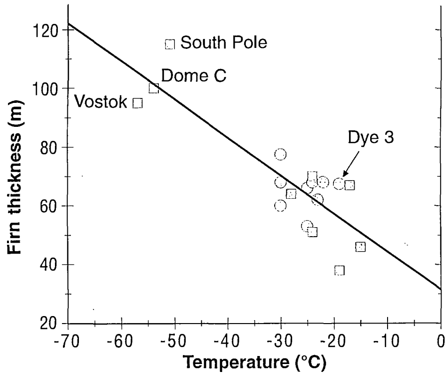

Fig. 1. Plot of observed values of firn thickness at Arctic (circles) and Antarctic (squares) polar-ice sites versus temperatures at a depth of 10 m. Data are from Paterson [(*3*), p. 15]. The firn temperatures are approximate mean annual surface temperatures on the ice sheets during snow accumulation. The linear fit is given by $Z = -1.307T + 31.5$.

We chose ^{84}Kr and ^{36}Ar for analysis because of their large ΔM (48 amu), their atmospheric ratio (1:48), which is attractive for precision mass spectrometry, and because both are noble gases. We used a noble gas machine with an effective radius of 54 cm (*7*) equipped with an in-line Daly multiplier followed by a normal Faraday collector. The ice samples, from a shallow core at the Dye 3 Greenland station, were drilled by our laboratory and the Polar Ice Core Operations (PICO) group in 1988 and stripped of gases shortly afterward in our laboratory.

Table 1 lists the measured ratio enrichments in the ice. Both δ^{15}N and δ^{18}O are essentially constant (at 0.24 and 0.54 per mil, respectively) in the approximate ratio expected for either fractionation process, showing the inability to distinguish between the two processes by N and O isotopes or by N_2, O_2, and Ar concentrations (*6*). The ^{84}Kr/^{36}Ar enrichments relative to free air have a mean value of 12.85 per mil, with a standard deviation of the mean (σ_m) of ±0.3 per mil for all measurements. ^{84}Kr/^{36}Ar enrichments are clearly much greater than predicted for effusional fractionation (5.9 per mil) and are much closer to, though somewhat less than, the calculated gravitational effect of 13.5 per mil (*6*). However, the best test for distinguishing the two processes is the relation between $\Delta(^{84}\text{Kr}/^{36}\text{Ar})$ and δ^{18}O because this ratio is independent of depth. Figure 2 shows this relation together with the predicted slopes of 24 for gravitational fractionation and 10.9 for effusional fractionation (*6*); these data confirm that gravitational equilibrium is the primary separation process in the firn column.

The data in Fig. 2 define an "effective depth" (Z_{eff}) for the observed gravitational

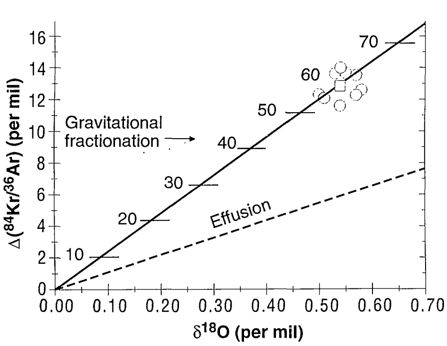

Fig. 2. Measurements of (^{84}Kr/^{36}Ar) versus ^{18}O in the Dye 3 ice core. The square marks the mean values. The solid line with a slope of 24 is the calculated relation for gravitational fractionation, with horizontal bars marking the expected firn-thickness increments (in meters) along the gravitational enrichment locus. The dashed line shows the expected relation for effusional fractionation, scaled to the mean ^{18}O value (*6*).

Isotope Laboratory, Scripps Institution of Oceanography, University of California at San Diego, La Jolla, CA 92093, USA.

*Present address: Division of Geological and Planetary Science, California Institute of Technology, Pasadena, CA 91125, USA.

Table 1. Isotopic enrichments in the Dye 3 Greenland ice core (65.2°N, 43.8°W). N_C is the number of ice-air comparisons (*7*); –, sample lost.

Z (m)	$\Delta(Ar/N_2)$ (per mil)	$\delta^{15}N$ (per mil)	$\delta^{18}O$ (per mil)	$\Delta(^{84}Kr/^{36}Ar)$ (per mil)	σ_m (per mil)	N_c	$\Delta(K/Ar)/\delta^{18}O$
72.05	3.9	0.17	0.50	12.32	2.2	5	24.64
84.23	1.6	0.22	0.53	13.63	2.6	10	25.71
94.84*	−0.1	0.29	0.55	13.67	0.6	6	24.85
94.84	−2.3	0.33	0.51	12.08	0.4	6	23.69
94.84	0.4	0.24	0.54	11.60	0.6	4	21.48
109.35	6.3	0.26	0.58	12.60	2.4	5	21.72
122.28	1.6	–	0.57	13.52	1.2	5	23.72
122.38	–	0.21	0.57	12.27	1.2	5	21.53
149.03	5.5	0.19	0.54	14.00	2.6	5	25.93
Mean	2.1	0.24	0.54	12.85	0.3		23.80
Air (1)†				−1.17	5.2	4	
Air (2)				0.14	0.5	3	
Air (3)				1.26	1.2	6	

*The 94.84-m $^{84}Kr/^{36}Ar$ ratios were measured on the Daly multiplier (versus all others on the Faraday collector). The smaller values of σ_m for the Daly measurements reflect the greater signal/noise ratio relative to samples measured on the Faraday collector. †Air samples processed through the ice extraction procedure.

enrichments, which is calculated from Eq. 1 to be 57.3 m for $\Delta(^{84}Kr/^{36}Ar)$ and 58.1 m for $\delta^{18}O$. The estimated firn thickness at Dye 3 is 65 to 70 m (*3*). The firn-ice transition can also be established by the loss of helium from core samples during the pumping out of air in the on-site He sampling system. Our measurements showed He losses of 99.5, 89, and 82% at core depths of 49, 64, and 73.5 m, respectively, and constant He concentration at 83 m and below; these data fix the firn-ice boundary at 77 ± 3 m. Thus, the effective depth of 57 m is 20 m less than the actual transition, or 74% of the true depth. We have proposed two mechanisms for this effect (*2*). First, there are transient mixing effects in the surficial firn layer caused by barometric pressure waves. Second, there is a small upward advection of air in the firn caused by compression, which can be calculated from the firn density-depth relation. The advective velocity is ~50 cm year^{-1} at the surface, decreasing to ~1 cm year^{-1} at 65 m, while the ratio of diffusive to advective fluxes increases from 0.16 at the surface to 1 at 40 m and to 24 at 68 m. This advective flux may also reduce the expected enrichment effect: a somewhat similar diminution of an isotope separation effect has been observed in the "carrier diffusion" process in the flow of gases through porous sandstone (*8*). However, given the high porosity in the uppermost firn layers, it is more likely that near-surface mixing by atmospheric pressure waves is the dominant effect.

Table 2. Predicted gravitational and solubility fractionation effects for a global cooling of 5°C, compared to the present gravitational effect at Dye 3. The Δ values (per mil) correspond to state 0 (firn: Z_{eff} = 57 m, T = −19°C; ocean + atmosphere = 5°C) and state 1 (firn: Z_{eff} = 100 m, T = −52°C; ocean + atmosphere = 0°C). The Δ_0(Grav) values are the predicted present Dye 3 gravitational effects scaled to the observed $^{84}Kr/^{36}Ar$ ratio by Eq. 1. $\Delta_{1/1}$(Grav) is the state 1 gravitational enrichment relative to the state 1 atmosphere; thus, Δ_0(Grav) − $\Delta_{1/1}$(Grav) is the change in gravitational enrichment assuming no changes in atmospheric ratios. $\Delta_{1/0}$(Atm) is the atmospheric ratio change from state 0 to state 1 calculated (Eq. 3) for oceanic solubility changes. $\Sigma\Delta_{1/0}$ is the total ratio enrichment in state 1 ice relative to the present state 0 atmosphere.

Ratio	ΔM	Δ_0 (Grav)	$\Delta_{1/1}$ (Grav)	$\Delta_{1/0}$ (Atm)	$\Sigma\Delta_{1/0}$
$O_2/^{40}Ar$	−8	−2.1	−4.3	−0.3	−4.6
$N_2/^{40}Ar$	−12	−3.2	−6.4	0.8	−5.6
$^4He/^{36}Ar$	−32	−8.5	−16.9	1.4	−15.6
$^{20}Ne/^{36}Ar$	−16	−4.2	−8.5	1.3	−7.2
$^{84}Kr/^{36}Ar$	+48	(12.85)	25.9	−2.6	23.3
$^{132}Xe/^{36}Ar$	+96	25.9	52.6	−9.3	42.8

Gravitational signals in ice caps reflect the ratio enrichments relative to the atmospheric composition at the time of firn accumulation, and because atmospheric ratios are themselves affected by global temperature variations through changes in the oceanic solubilities of gases, the solubility effects modulate the gravitational effects relative to present-day air to some extent. The solubility effects are difficult to calculate because of horizontal and vertical temperature gradients in the atmosphere and the ocean and their variations with climatic change. For a first approximation we used a simple model of an atmosphere and ocean in isothermal equilibrium, in which the atmosphere is contained in a finite volume, V_A, and partitioning of gases is scaled by the ratio of V_A to the volume of seawater, V_S. In this system, the atmospheric content of a gas N for two system-temperatures T_0 and T_1 is given by

$$N_1/N_0 = \frac{[V_A/V_S + (\beta_0 T_0/T^+)]}{[V_A/V_S + (\beta_1 T_1/T^+)]} \qquad (3)$$

where β is the Bunsen solubility coefficient (volume/volume), V_A = 800 liters per square centimeter of Earth's surface (the finite atmospheric volume that would contain the atmospheric gases at P = 1 atm), V_S = 269 liters per square centimeter of Earth's surface (so that $V_A/V_S = 3$), and T^+ = 273 K. Using the β values (*9*), we calculated the changes in atmospheric content resulting from a global temperature change from 5°C (state 0) to 0°C (state 1) (*10*): N_2, −0.55 per mil; O_2, −1.68 per mil; Ar, −1.35 per mil; Kr, −3.9 per mil; and Xe, −10.6 per mil (He and Ne, <0.1 per mil).

Table 2 compares the gravitational and solubility effects on various ratios for a global cooling of 5°C from state 0 to state 1. The firn parameters (Z_{eff} and T) are the present Dye 3 values (57 m and −19°C) for state 0, and 100 m and −52°C for state 1 (*11*). The atmospheric effect of increased solution in the ocean, $\Delta_{1/0}$(Atm), is ~10% of the state 1 gravitational enrichment, $\Delta_{1/1}$(Grav), for all ratios except $^{20}Ne/^{36}Ar$ and $^{132}Xe/^{36}Ar$, for which the atmospheric changes are ~16.5% of the gravitational effects. While the total changes in O_2/Ar and N_2/Ar ratios are essentially unmeasurable, the Kr/Ar and Xe/Ar state 1 versus state 0 enrichments, $\Sigma\Delta_{1/0}$, are 10.4 and 17 per mil. It is apparent that for the simple model used here, measurements of the total state 1 Kr and Xe enrichments in an ice sample ($\Sigma\Delta_{1/0}$), together with the known ratios of Kr to Xe gravitational enrichment effects (which are independent of firn depth and temperature) and the mean β ratios, can be used to calculate precisely the state 1 firn thickness and surface ice-sheet temperature. Of course, the actual global system is much more complex than our simple model, but the availability of four noble gas pairs provides a rich matrix of data that can be used to model the gravitational and solubility effects in conjunction with models of global temperature variations that incorporate temperature changes of polar ice cap surfaces as related to mean global temperatures.

REFERENCES AND NOTES

1. Y. Horibe, K. Shigehara, C. C. Langway Jr., *Earth Planet. Sci. Lett.* **73**, 207 (1985).
2. H. Craig, Y. Horibe, T. Sowers, *Science* **242**, 1675 (1988); H. Craig, *ibid.* **262**, 763 (1993).
3. Data are from W. B. Paterson, *The Physics of Glaciers* (Pergamon, Oxford, ed. 3, 1994). The firn thicknesses were established by density measurements on cores from 18 Arctic and Antarctic sites. Although there is considerable scatter in the estimated transition depths (which are difficult to measure precisely), the data show that $dZ/dT \approx -1.30$ m °C^{-1} (Fig. 1).
4. J. W. Gibbs, *Collected Works*, vol. 1, *Thermodynamics* (Yale Univ. Press, New Haven, 1928).
5. The δ values (per mil) are equal to $10^3 \times [(R/R_A) - 1]$, where R is the isotopic or atomic ratio and R_A is the atmospheric ratio. We use δ for isotopic enrichments and Δ for enrichments of atomic or molecular ratios.
6. It was previously shown (*2*) that the observed heavy isotope enrichments could also be produced by molecular effusion from compressed air bubbles in the

basal firn layer, coupled to removal of gases by vertical advection of air caused by compression of the firn. The effusional enrichment ratio for two isotopes is controlled by the kinetic fractionation factor $\alpha = (M/M_i)^{1/2}$, and the resulting isotope enrichment is given by the Rayleigh equation:

$$R/R_0 = (1 - F_L)^{\alpha-1}$$

where F_L is the fraction of component N lost by effusion through a molecular leak. Because effusional enrichment depends on the fractional gas loss, the expected gravitational and effusional enrichments cannot be compared unless F_L is specified. We used the mean $^{18}O/^{16}O$ enrichment in the ice samples to calculate a fictive value of 1.79% for $F_L(O_2)$ and then scaled the F_L values for other components to $F_L(O_2)$. Thus, $[1 - F_L(j)] = [1 - F_L(O_2)]^{\alpha(j)}$, where $\alpha(j) = (M_{O_2}/M_j)^{1/2}$, the fractionation factor for any component j versus O_2. The resulting F_L values (1.91% for N_2 and 1.69% for ^{36}Ar) were then used to calculate the other effusional ratio enrichments, scaled to $F_L(O_2)$. The effusional and gravitational enrichments ($Z = 60$ m, $T = -20$°C) for the various ratios are as follows:

Component	Δ(Eff) per mil)	Δ(Grav) (per mil)
$\delta^{15}N$	0.33	0.28
$\delta^{18}O$	0.54	0.56
$\delta^{40}Ar$	0.87	1.12
$\Delta(O_2/N_2)$	1.24	1.11
$\Delta(Ar/N_2)$	3.14	3.35
$\Delta(^{84}Kr/^{36}Ar)$	5.90	13.50
$\Delta(^{132}Xe/^{36}Ar)$	8.18	26.85

The gravitational and effusional ratio enrichments are indistinguishable within limits of analytical accuracy for all these ratios, with the exception of the $^{84}Kr/^{36}Ar$ and $^{132}Xe/^{36}Ar$ pairs, for which the gravitational enrichments are 2.3 and 3.3 times the calculated effusional effects, respectively. Moreover, the predicted ratio of $^{84}Kr/^{36}Ar$ to $^{18}O/^{16}O$ enrichments is 24.1 for gravitational separation versus only 10.9 for effusion. Note that the effusional enrichment ratio is constant over the range of Fig. 2 because, to first order, the ratio is simply $\alpha(36/32)[\alpha(84/36) - 1]/[\alpha(34/32) - 1] = 10.9$. (Here, the mass numbers are used only as labels for the individual fractionation factors.)

7. See H. Craig, K. Marti, R. Wiens, *A Static Mass Spectrometer with Triple Collection for Nitrogen and Neon Isotopes* (Scripps Institution of Oceanography Tech. Rep. 93-11, 1993) for details of the Kr/Ar ratio analyses. Gases trapped in bubbles were extracted by melting ice samples (~30 g) in a high-vacuum system, after which aliquots were taken for various analyses. For the noble gas measurements, sample analyses were alternated with measurements on the on-line machine air standard, and all measurements were made at the same ^{36}Ar ion beam intensity. Three samples of air were put through the extraction procedures and analyzed with the ice samples; Table 1 shows that the observed ratios were indistinguishable from the machine air standard. The stable isotope ratios were measured on a 10-inch-radius, triple-collection mass spectrometer (SAMSON). The gases were cycled over a hot carbon filament to convert O_2 to CO_2 for the mass spectrometer, and the remaining N_2-Ar fraction was introduced into the spectrometer through I_2O_5 reagent to remove all traces of CO. The Ar/N_2 ratios were measured by conventional gas chromatography (GC); although these ratios are accurate to only ~5 per mil in our GC system, they are important because it was previously shown (2) that large negative enrichments in both Ar/N_2 and O_2/N_2 can be caused by loss of gases from ice through microfractures, due to differential capillary effects during pumping. The measured Ar/N_2 ratios are consistent with enrichments expected for either gravitational or effusional fractionation and show no significant effect of possible gas loss.
8. H. Craig, *Science* **159**, 93 (1968).
9. R. F. Weiss, *Deep-Sea Res.* **17**, 721 (1970); *J. Chem. Eng. Data* **16**, 235 (1971); D. Wood and R. Caputi, *U.S. Naval Radiol. Defense Lab. Tech. Pub. USNRDL-TR-988* (1966).
10. M. Stute, P. Schlosser, J. F. Clark, W. S. Broecker, *Science* **256**, 1000 (1992). The 5°C global cooling during the last glacial maximum is based on the noble gas geothermometer (using Ne, Kr, and Xe) for ground water. (The temperatures obtained by this method need corrections for the solubility effects on atmospheric partial pressures.)
11. K. M. Cuffey *et al.*, *Science* **270**, 455 (1995). The −52°C temperature estimate for central Greenland is based on fitting ice-core ^{18}O data to a borehole temperature model.

12. We thank J. Welhan and the members of the PICO group for drilling the Dye 3 ice core, D. Burtner for laboratory assistance, K. Turekian for discussion, and C. C. Langway Jr. for his interest in and enthusiasm for our ice-core work. R. Keeling pointed out to us that atmospheric concentrations will be affected by global temperature changes. Supported by the Polar Programs Office of NSF.

13 July 1995; accepted 17 January 1996

River Meandering as a Self-Organization Process

Hans-Henrik Stølum

Simulations of freely meandering rivers and empirical data show that the meandering process self-organizes the river morphology, or planform, into a critical state characterized by fractal geometry. The meandering process oscillates in space and time between a state in which the river planform is ordered and one in which it is chaotic. Clusters of river cutoffs tend to cause a transition between these two states and to force the system into stationary fluctuations around the critical state.

The meandering river system is characterized by recurrent river planform patterns, repeated with little variation from one river to the next irrespective of their magnitude and from one scale to another within each river. This consistency suggests that a higher level of processes forms by self-organization from the physical processes of deposition and erosion operating in the system. These physical processes may be described by continuum fluid mechanics. Although meandering dynamics can be simulated from models based on continuum mechanics, such models reveal little about the holistic, spatiotemporal properties of the meandering process, for example, the hierarchical, fractal geometry of the river planform. [Self-affine fractal scaling of meandering river planforms was first suggested in (*1*) and has been analyzed in (*2, 3*).] It has therefore been suggested that meandering needs to be understood in terms of chaotic dynamics and self-organization (*4*–*6*). In this report, I use a fluid mechanical model developed by Parker, Howard, and co-workers (*7, 8*) to explore the dynamical properties of meandering by simulation.

Meandering is caused by the operation of two opposing processes (*4*), which are linked by a complex feedback that is partly under local geometrical control: lateral migration acts to increase sinuosity, whereas cutoffs (the formation of oxbow lakes) act to decrease it. Lateral migration results from bend erosion and deposition (*4, 9*). Cutoffs arise from a local geometry (Kinoshita shape), which is created by the lateral migration process (*4, 10, 11*).

The state of the system is conveniently measured by the dimensionless parameter sinuosity

$$s = L/\ell$$

where L is the length of the river along its course between two points and ℓ is the shortest length between the same points. The quantities L and ℓ are measured in units of average width, w. When the river is straight, sinuosity has a minimum value of 1. In principle, no maximum value exists. Sinuosity is related to the information content and symmetry of the system (*5*). Oxbow lakes have a finite length range, with a minimum value of ≈7 and a maximum of ≈$40w$.

In the simulations (Fig. 1, A and B), the river typically formed two coexisting domains, one with consistently high sinuosity (mean $s \approx 3.5$) and one with consistently low sinuosity (mean $s \approx 2.7$). Because a straight line is the most ordered state the river can take (zero entropy, perfect axial symmetry), the low-sinuosity regions represent a distinctly more ordered state than the high-sinuosity regions (weak versus strong asymmetry).

The low-sinuosity domains in Fig. 1, A and B, formed as a result of a clustering of cutoff events. Each cutoff has a tendency to trigger other cutoffs in its vicinity by causing accelerated local change, and this may generate a cluster of cutoffs in space and time. Similarly, in natural rivers, successive cutoffs occur only rarely with the same spacing or at regular intervals, and so clusters are formed.

When the simulated river was locally straightened by cutoffs, the dynamics died down to create a window of slow change that persisted for awhile, before a gradual

---

Department of Earth Sciences, University of Cambridge, Cambridge CB2 3EQ, UK.